APPLIED SCIENCES AND ENGINEERING

A polyvalent vaccine for selectively killing tumor-associated bacteria to prevent cancer metastasis

Zheyu Kang[1]†, Linfu Chen[1]†, Pengxing Li[1], Zixuan Zheng[2], Jingjing Shen[1], Zhisheng Xiao[1], Yu Miao[1], Yang Yang[2,3,4], Qian Chen[1]*

Specific bacteria, including *Fusobacterium nucleatum*, *Streptococcus sanguis*, *Enterococcus faecalis*, and *Staphylococcus xylosus*, have been identified as contributors to breast cancer metastasis. Due to limitations such as lack of selectivity, traditional antibiotic therapies face obstacles in eliminating intratumoral bacteria. Herein, this work proposes the use of therapeutic vaccines to selectively target and eliminate harmful bacteria within tumors. A multivalent vaccine encapsulating both insoluble and soluble bacterial antigens was developed, addressing the shortcomings of traditional antibacterial vaccines by balancing broad antigen coverage with effective immune activation. This vaccine induces robust downstream immune responses to eliminate *F. nucleatum*, *S. sanguis*, *E. faecalis*, and *S. xylosus*, demonstrating notable therapeutic and preventive efficacy in bacteria-induced cancer metastasis models. Unexpectedly, vaccinated infected mice showed even slower tumor metastasis than uninfected mice. Overall, this study validates the potential of nanovaccines in modulating the intratumoral microbiome for tumor therapy and highlights tumor-associated bacterial infections as potential promising antitumor targets.

INTRODUCTION

Breast cancer has emerged as one of the most prevalent malignancies globally, ranking among the most diagnosed cancers and a leading cause of cancer-related mortality in women (*1*). While early-stage breast cancer, such as ductal carcinoma in situ, can be effectively managed through interventions such as surgical resection, the inherent loose cohesion between breast cancer cells and the intricate network of lymphatic and blood vessels within breast tissue facilitates the detachment and subsequent dissemination of cancer cells to distant organs, including the lungs, liver, and bones (*2*). This metastatic journey signifies a transition to a more formidable phase of breast cancer, complicating treatment efforts and dimming the prospects for a favorable outcome (*3*, *4*). Consequently, beyond the pivotal role of early detection and intervention, thwarting the metastatic progression of breast cancer is of paramount importance.

The human microbiome represents an immense ecosystem, with its collective genetic content surpassing that of the human genome by more than 150-fold (*5*). These microbiomes, resisting across various bodily niches, play critical roles in both the healthy functioning and disease states of their host (*5*). Recent findings have illuminated the presence of microorganisms within tumors, including but not limited to colorectal, pancreatic, and lung cancers, revealing the diverse bacterial profiles associated with different cancer types (*6*). The microbial inhabitants of tumor tissues significantly influence cancer susceptibility, disease progression, and therapeutic outcomes (*7*–*9*). Specifically, in breast cancer tissues, the colonization by bacteria such as *Fusobacterium nucleatum*, *Streptococcus sanguis*, *Enterococcus faecalis*, and *Staphylococcus xylosus* has been detected (*10*–*12*). Investigation into their roles has demonstrated that these microorganisms can promote breast cancer metastasis through mechanisms such as impeding the recruitment of tumor-infiltrating T cells or enhancing the cytoskeletal resistance to fluid shear stress in tumor cells (*11*). This burgeoning field of research underscores the intricate interplay between the microbiome and cancer, highlighting potential avenues by regulating bacteria for innovative therapeutic strategies.

Antibiotics, traditionally used to eradicate bacteria, can directly eliminate or suppress bacteria proliferation (*13*). Nonetheless, deploying antibiotics to expunge bacteria within cancer tissue is fraught with challenges. Humans are continuously exposed to environments harboring bacteria capable of colonizing tumors, necessitating persistent antibiotic therapy for the duration of tumor's presence to prevent these bacteria from growing within the tumor (*14*). This protracted use of antibiotics is particularly inadvisable due to several critical concerns. First, the potential side effects of antibiotics, including hepatorenal toxicity, hypersensitivity reactions, and other systemic effects, cannot be overlooked (*15*). Second, antibiotics do not discriminate between pathogenic and symbiotic bacteria, leading to dysbiosis of the gut microbiota (*16*–*18*). This disruption can manifest in gastrointestinal disturbance, such as diarrhea and a compromised immune system, which can significantly attenuate the effectiveness of cancer immunotherapies such as programmed cell death protein 1 (PD-1) inhibitors, thus tipping the balance toward detriment rather than benefit (*19*, *20*). Moreover, the injudicious use of antibiotics may inadvertently fuel the rise of "superbugs" within clinical settings, posing a grave public health risk (*21*, *22*).

To circumvent the challenges associated with antibiotic, we propose an innovate therapeutic strategy using vaccines to eliminate intratumoral bacteria, which aims to selectively target specific bacteria and provide long-term protection. Naturally, the uptake and presentation of intratumoral bacterial antigens (Ags) by immune cells are minimal, which often results in immune evasion by these bacteria (*23*). Delivering intratumoral bacterial Ags to the immune system via vaccines can activate an immune response and normalize the immune surveillance against these bacteria (*24*). An ideal anti-intratumoral bacterial vaccine should achieve the dual objectives of

[1]Institute of Functional Nano and Soft Materials (FUNSOM), Jiangsu Key Laboratory for Carbon-Based Functional Materials and Devices, Soochow University, Suzhou 215123, China. [2]Department of Thoracic Surgery, Shanghai Pulmonary Hospital, School of Medicine, Tongji University, Shanghai 200433, China. [3]Central Laboratory, Shanghai Pulmonary Hospital, School of Medicine, Tongji University, Shanghai 200433, China. [4]School of Materials Science and Engineering, Tongji University, Shanghai 201804, China.
*Corresponding author. Email: chenqian@suda.edu.cn
†These authors contributed equally to this work.

clearing bacteria and eliminating infected tumor cells (*25*, *26*). The key to an antibacterial immune response lies in activating humoral immunity to produce antibodies that neutralize bacteria, while the key to eliminate infected tumor cells lies in activating cellular immunity to enable cytotoxic T cells to kill these cells (*27*, *28*). RNA vaccines and peptide vaccines can induce robust cellular immunity, but their limited number of target proteins makes them unsuitable for bacteria with diverse protein (*29*, *30*). Inactivated vaccines with aluminum adjuvant, commonly used as bacterial vaccines, contain multiple bacterial Ags and can activate robust humoral immunity but have limited effects on cellular immunity (*31*). Therefore, there is an urgent need for a therapeutic vaccine that can cover a broad spectrum of bacterial Ags while eliciting potent cellular immunity.

To selectively target and eliminate bacteria within breast tumor cells and thereby suppress bacteria-induced breast cancer metastasis, we have developed a safe and effective quadrivalent therapeutic vaccine [poly(lactic-*co*-glycolic acid)/Ags]. This innovative vaccine encapsulates both water-soluble and water-insoluble components of sonicated lysates from *F. nucleatum*, *S. sanguis*, *E. faecalis*, and *S. xylosus*—the four most common metastasis-promoting bacteria found in human cancer tissues—into PLGA nanoparticles, which exhibit excellent biocompatibility (*32*, *33*). As a result, the vaccine boasts a highly abundant repertoire of bacterial Ags. The obtained PLGA/Ags are appropriately sized for lymph node accumulation following intradermal injection, where they are efficiently taken up by dendritic cells (DCs). Within these cells, the nanoparticles release their antigenic cargo, promoting DC maturation and Ag presentation, thereby eliciting robust humoral and cellular immunity against bacteria. In a bacteria-induced mouse breast cancer lung metastasis model, PLGA/Ags could successfully eradicate intratumoral bacteria and suppress breast cancer metastasis, doubling the survival time of mice with bacteria infected tumors. Due to the cellular immune cytotoxicity against infected tumors, mice treated with PLGA/Ags vaccine even exhibited longer survival compared to those with uninfected tumor. Furthermore, PLGA/Ags could induce potent immune memory effect, providing long-term protection against bacteria-induced breast cancer metastasis (Fig. 1). We also applied this vaccine in a bacteria-induced colon cancer metastasis model and verified that its efficacy can extend to other types of tumors. Together, the quadrivalent therapeutic vaccine developed here, characterized by a straightforward manufacturing process, robust immunogenicity, and excellent biocompatibility, holds promise

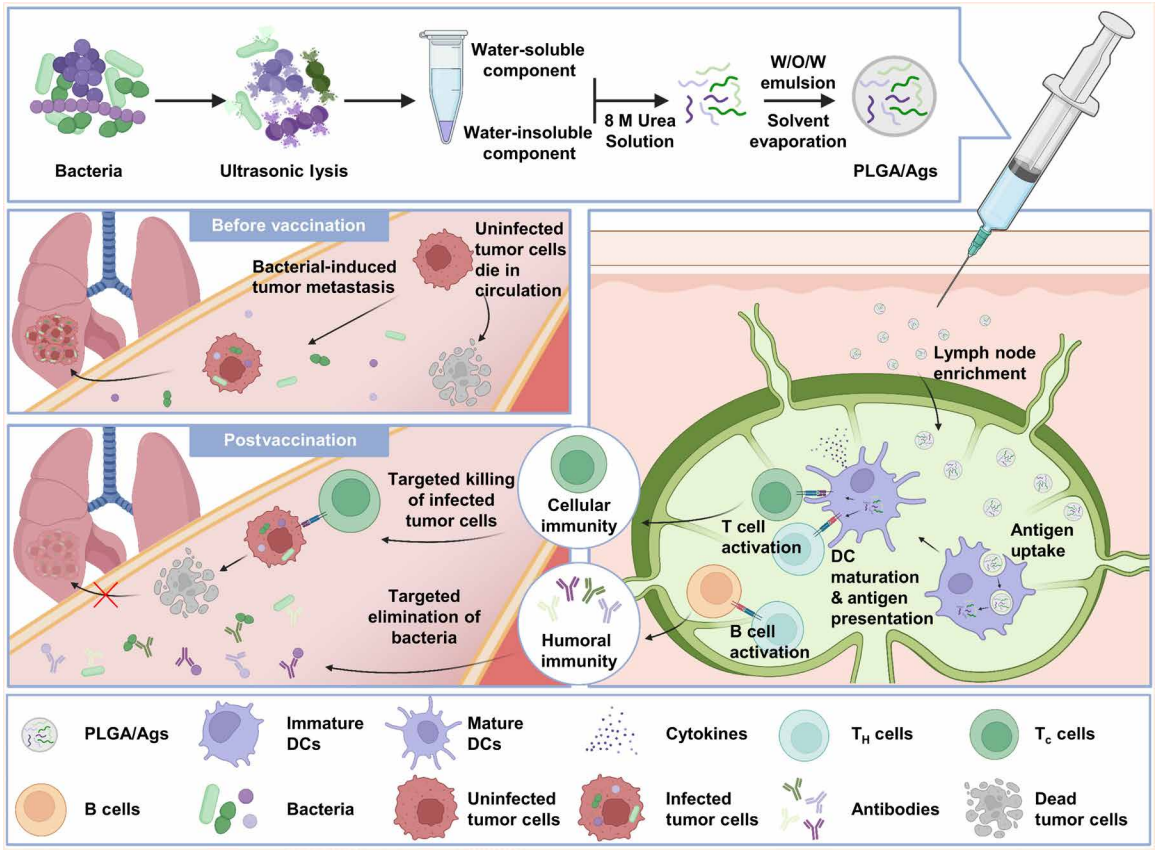

Fig. 1. The schematic illustrates that the antibacterial immune response induced by PLGA/Ags vaccine effectively prevents bacteria-induced tumor metastasis. The PLGA/Ags vaccine is prepared by encapsulating with both water-soluble and water-insoluble bacterial lysate into a PLGA shell, providing a broad spectrum of Ags. Upon intradermal injection, these nanoparticles efficiently accumulate in the lymph nodes, facilitating DC maturation and antigen presentation, which subsequently triggers robust cellular and humoral immune responses. While uninfected tumor cells are prone to death in circulation, tumor cells infected by *F. nucleatum*, *S. sanguis*, *S. xylosus*, and *E. faecalis* can survive in the bloodstream and metastasize to other organs. Postvaccination, the specific $CD8^+$ cytotoxic T lymphocyte response can eradicate the infected tumor cells, and the humoral immunity can clear the bacteria, thereby preventing tumor cell metastasis. T_H cells, T helper cells; T_c cells, cytotoxic T cells. Created with BioRender.com.

for selectively eliminating intratumoral bacteria and preventing cancer metastasis in patients with bacterial infections.

RESULTS

Preparation and characterization of PLGA/Ags

To engineer a therapeutic vaccine adept at selectively eradicating specific bacterial populations within tumor environment, we meticulously designed PLGA nanoparticles encapsulating lysates from *F. nucleatum*, *S. sanguis*, *E. faecalis*, or *S. xylosus*. This approach was underpinned by the objective to emulate natural infection dynamics, thereby eliciting a comprehensive and enduring immune response (*34*). Opting for lysates replete with a wide array of proteins from four bacteria served to furnish a rich antigenic palette. To extend the spectrum of antigenic coverage, the bacteria were lysed by ultrasonication in an 8 M urea solution, which was chosen for its superior efficiency in enhancing the solubility of insoluble proteins (*35*). Subsequently, analyses including bicinchoninic acid (BCA) assay and SDS–polyacrylamide gel electrophoresis (PAGE) were carried out to confirm that bacterial lysates prepared in the 8 M urea solution exhibited higher protein concentrations and broader protein profile compared to those prepared in phosphate-buffered saline (PBS) solutions (Fig. 2, A and B).

Then, the obtained bacterial lysates were encapsulated into PLGA nanoparticles (PLGA/Ags) using a double-emulsion technique followed by solvent evaporation. Different feed ratios of PLGA and bacterial lysates were tested (table S1), with the final formulation chosen on the basis of a bacterial Ag loading capacity of 3.33%. The resultant nanoparticles were measured by dynamic light scattering (DLS), which revealed a hydrodynamic diameter of ~200 nm (Fig. 2C). To ensure effective Ag delivery to Ag-presenting cells (APCs), it is essential that vaccine nanoparticles maintain stability under in vivo conditions and prevent the premature release of Ags into body fluids. To investigate the stability of PLGA/Ags, it was incubated in PBS at

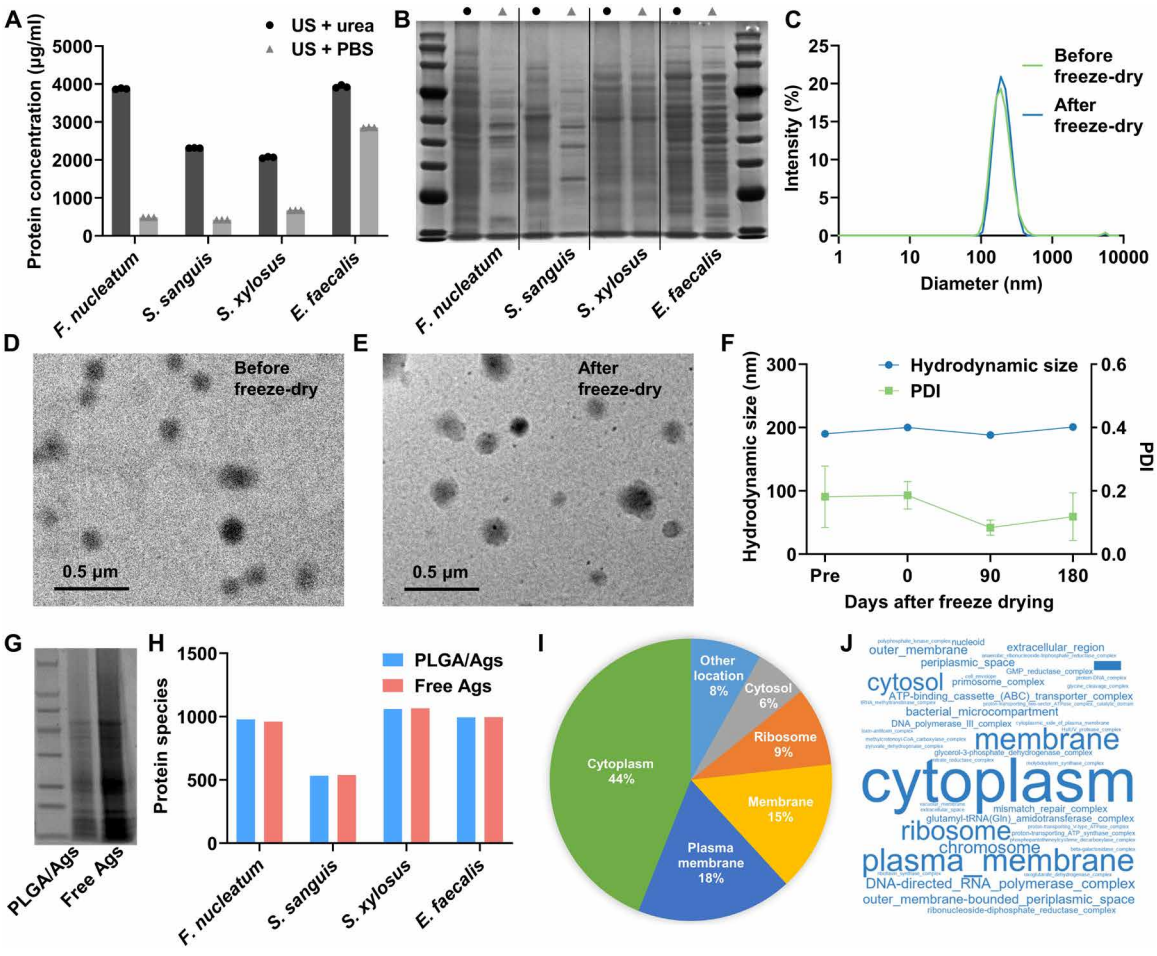

Fig. 2. Preparation and characterization of PLGA/Ags nanovaccines. (**A**) Protein concentration of lysates obtained from *F. nucleatum*, *S. sanguis*, *E. faecalis*, and *S. xylosus* after sonication in urea and PBS solutions. US, Ultrasonic lysis. (**B**) SDS–polyacrylamide gel electrophoresis (PAGE) analysis of proteins from markers, and ultrasonic lysates of *F. nucleatum*, *S. sanguis*, *E. faecalis* and *S. xylosus* in urea and PBS solutions. (**C**) Hydrodynamic sizes of PLGA/Ags nanoparticles before and after freeze-dry. (**D** and **E**) Transmission electron microscopy (TEM) images of PLGA/Ags nanoparticles before and after freeze-drying (scale bars, 0.5 μm). (**F**) Time-lapse hydrodynamic size and PDI of PLGA/Ags after freeze-drying. Data are presented as the means ± SD ($n = 3$). (**G**) SDS-PAGE analysis of proteins before and after encapsulation in PLGA. (**H**) Number of protein species detected by liquid chromatography–mass spectrometry (LC-MS) in *F. nucleatum*, *S. sanguis*, *E. faecalis*, and *S. xylosus* before and after encapsulation in PLGA. (**I**) Proportions of primary subcellular locations of proteins from PLGA/Ags nanoparticles. (**J**) Word cloud illustrating subcellular locations of proteins from PLGA/Ags nanoparticles.

37°C for 21 days. No significant changes were observed in the average hydrodynamic size and the polydispersity index (PDI) (fig. S1), indicating that the formulation remains stable under conditions that closely resemble the in vivo environment. Subsequently, transmission electron microscopy (TEM) provided detailed imaging to confirm the homogenous size distribution and spherical morphology of PLGA/Ags (Fig. 2D). Recognizing the logistical challenges posed by the necessity for cold chain management in current vaccine dissemination, which can impede global accessibility, there is a pressing need to forge vaccines amenable to room temperature storage (*36*, *37*). In our endeavor to surmount this hurdle, sucrose was used as a cryoprotectant during the freeze-drying process of PLGA/Ags (*38*). As shown in Fig. 2 (C and E), DLS and TEM analyses indicated that the lyophilization and reconstitution did not affect the size and morphology of the PLGA/Ags nanoparticles. Moreover, the average hydrodynamic size and PDI of the PLGA/Ags remained consistency after freeze-drying and subsequent reconstitution, even after intervals of 90 and 180 days (Fig. 2F), demonstrating the exceptional stability of PLGA/Ags at ambient conditions, heralding implications for storage and distribution without reliance on cold chain logistics.

To evaluate whether various bacterial proteins are all encapsulated in PLGA, SDS-PAGE was performed. As shown in Fig. 2G, a direct correlation was observed between the protein bands from the bacterial lysate and those evident in the PLGA encapsulated group, indicating the successful entrapment of a diverse array of proteins derived from the bacterial lysates within the PLGA nanoparticles. Furthermore, a comprehensive proteomic analysis using liquid chromatography with tandem mass spectrometry (LC-MS/MS) identified a total 3642 proteins in the PLGA/Ags complexes. These results confirmed that the protein profile of PLGA encapsulates mirrors that of the original bacterial lysates, encompassing an extensive spectrum of proteins from each bacterium species (Fig. 2H). Further insights gained from the subcellular localization analysis of the proteins identified by LC-MS/MS indicated that these predominantly hail from the cytoplasm, plasma membrane, membrane, and ribosomes, suggesting that the antigenic repertoire within the PLGA nanoparticles comprehensively represents bacterial proteins across various cellular domains (Fig. 2, I and J). Because *F. nucleatum*, *S. sanguis*, *E. faecalis*, and *S. xylosus* are intracellular bacteria, proteins at various locations within these bacteria can be processed by tumor cells and presented on the cell surface via major histocompatibility complex I (MHC I). Using PLGA/Ags to activate immune responses that cover a broad range of Ags can generate diverse $CD8^+$ T cells targeting these Ags, thereby reducing immune evasion by tumor cells harboring these bacteria.

In vitro immune stimulation by PLGA/Ags

For a therapeutic vaccine, the capacity to activate DC maturation is crucial for Ag presentation and subsequent immune system engagement (*39*). Therefore, in vitro assessments of the influence exerted by PLGA/Ags complexes on DC maturation were conducted (Fig. 3A). Before the principal investigations, we ascertained the biosafety profile of our PLGA/Ags formulation. At the protein concentration up to 250 μg/ml, the DC2.4 cells still maintained good viability in the presence of PLGA/Ags (fig. S2), indicating the successful mitigation of potential cytotoxic components, such as lipopolysaccharides (LPSs) in the bacterial lysates, during the encapsulation process. For the maturation of DCs in vitro, bone marrow–derived DCs (BMDCs) exposed to PLGA/Ags demonstrated the most marked elevation in the expression of co-stimulatory molecules (CD80 and CD86) compared to both the untreated and free Ag–treated cells (Fig. 3, B and C). Additionally, BMDCs in the company of PLGA/Ags secreted significantly higher levels of pro-inflammatory cytokines, including interleukin-12p70 (IL-12p70), tumor necrosis factor–α (TNF-α), and IL-6 (Fig. 3, D to F). Additionally, PLGA/Ags nanoparticles subjected to long-term lyophilization were shown to retain their ability to effectively promote DC maturation (fig. S3, A and B). This superior performance of PLGA/Ags in stimulating DC maturation may be attributed to the augmented internalization of nanoparticles (*40*). We then investigated the internalization of free Ags and PLGA/Ags by DC2.4 cells. As illustrated in Fig. 3 (G and H), the Ag internalization by DCs was substantially higher in the PLGA/Ags group than that in the free Ags group, a gap that widened with time. Considering that the activation of the immune response hinges not only on the Ag acquisition but also on the processing and presentation of these Ags (*41*), we used confocal microscopy to track the journey of fluorescein isothiocyanate (FITC)–labeled Ags within DCs. Between 4 and 8 hours, there was a progressive intensification of the Ag signal, which coalesced with the lysosome signal. From 12 to 24 hours, we observed Ags breaking free from lysosomal confines and arranging themselves on the cell surface in a ring-like pattern (Fig. 3I and fig. S4). At each observed time point, the Ag signals in the PLGA/Ags group overshadowed that in the free Ags group, indicating that Ags loading onto PLGA nanoparticles effectively increased Ag uptake and presentation by DCs.

To delve deeper into the mechanism of immune activation induced by PLGA/Ags, we conducted transcriptome sequencing on BMDCs cultured alongside either PLGA/Ags or PBS for comparative analysis. Genes implicated in BMDC maturation, including those coding for TNFs, ILs, chemokines, and their receptors, were significantly up-regulated after PLGA/Ags treatment (Fig. 3J). In addition, through Kyoto Encyclopedia of Genes and Genomes pathway enrichment analysis, it was found that the up-regulated differentially expressed genes were predominantly concentrated in pathways such as Toll-like receptor (TLR) signaling, nuclear factor κB signaling, C-type lectin receptor signaling, and nucleotide oligomerization domain–like receptor signaling (Fig. 3K), revealing that the activation of BMDCs induced by PLGA/Ags is a composite process involving multiple signaling cascades. Furthermore, gene ontology analysis revealed that the up-regulated differential expression genes were highly associated with processes including T cell activation, T helper 1–type immune response and the secretion of inflammatory cytokines (Fig. 3L), suggesting that the DCs activated by PLGA/Ags have the enhanced capability to efficiently activate downstream immune response.

In vivo immune stimulation by PLGA/Ags

Different from the in vitro experiments where nanoparticles can directly interact with DCs in substantial quantities, Ags administrated intradermally must navigate to the draining lymph nodes (dLNs) to engage with DCs (*42*). Before investigating the immune response elicited by the PLGA/Ags vaccine, its transportation efficacy to the dLNs was scrutinized. As shown in Fig. 4 (A to C), sequential imaging of BALB/c mice, intradermally injected with either PLGA/Ag-Cy5.5 or free Ag–Cy5.5, revealed distinct patterns over time. The fluorescence intensity within the inguinal dLNs of mice injected with PLGA/Ag-Cy5.5 markedly increased, peaking at 8 hours and subsequently diminishing, yet remained discernible up to 36 hours postinjection. Conversely, the fluorescence intensity in the inguinal dLNs

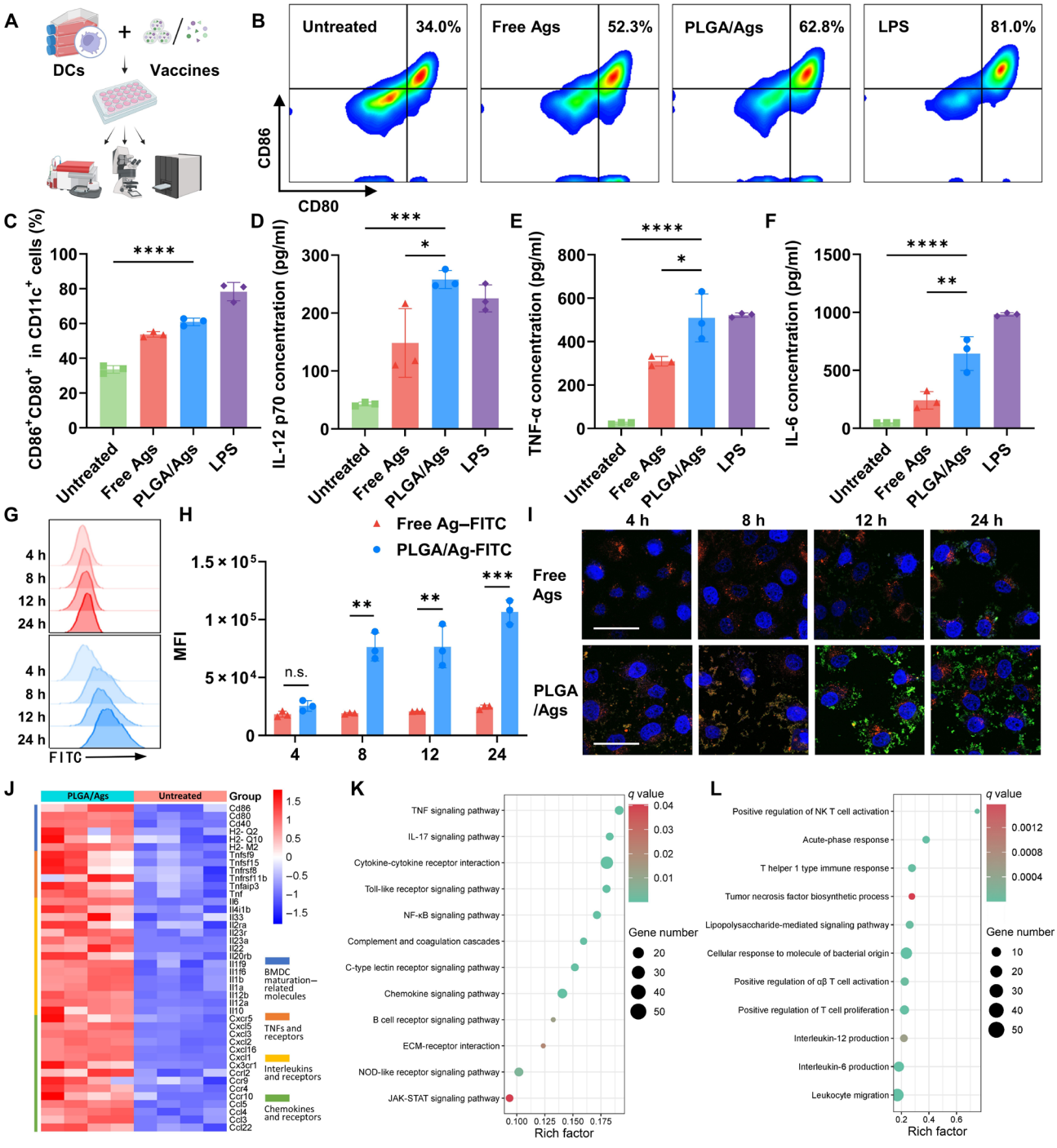

Fig. 3. In vitro DC uptake and activation. (**A**) Schematic representation of the experimental setup for DC uptake and activation. Created with BioRender.com. (**B** and **C**) Representative flow cytometric plots (B) and statistical analysis (C) showing the maturation of BMDCs in different groups. Data are presented as means ± SD ($n = 3$). (**D** to **F**) Secretion levels of interleukin-12p70 (IL-12p70) (D), tumor necrosis factor–α (TNF-α) (E), and IL-6 (F) by BMDCs in different groups. Data are presented as means ± SD ($n = 3$). (**G** and **H**) Representative flow cytometric plots (G) and statistical analysis (H) of mean fluorescence intensity (MFI) in DC2.4 cells incubated with fluorescein isothiocyanate (FITC)–labeled free Ags or PLGA/Ags for different time points. Data are presented as means ± SD ($n = 3$). (**I**) Confocal fluorescence images of DC2.4 cells incubated with FITC-labeled (green) free Ags or PLGA/Ags for different time points. Nuclei and lysosomes were stained with 4′,6-diamidino-2-phenylindole (DAPI; blue) and LysoTracker (red), respectively (scale bars, 40 μm). h, hours. (**J**) Heatmap showing the transcript expression of the related genes in BMDCs incubated with PLGA/Ags or PBS. (**K**) Kyoto Encyclopedia of Genes and Genomes pathway analysis based on differentially expressed genes between the PLGA/Ags and untreated groups. NF-κB, nuclear factor κB; ECM, extracellular matrix; NOD, nucleotide oligomerization domain; JAK-STAT, Janus kinase–signal transducer and activator of transcription. (**L**) Gene ontology analysis based on differentially expressed genes. Statistical significance was calculated via one-way analysis of variance (ANOVA) [(C) to (F)] and unpaired *t* test (H) in GraphPad Prism. NK, natural killer; *$P < 0.05$; **$P < 0.01$; ***$P < 0.001$; ****$P < 0.0001$.

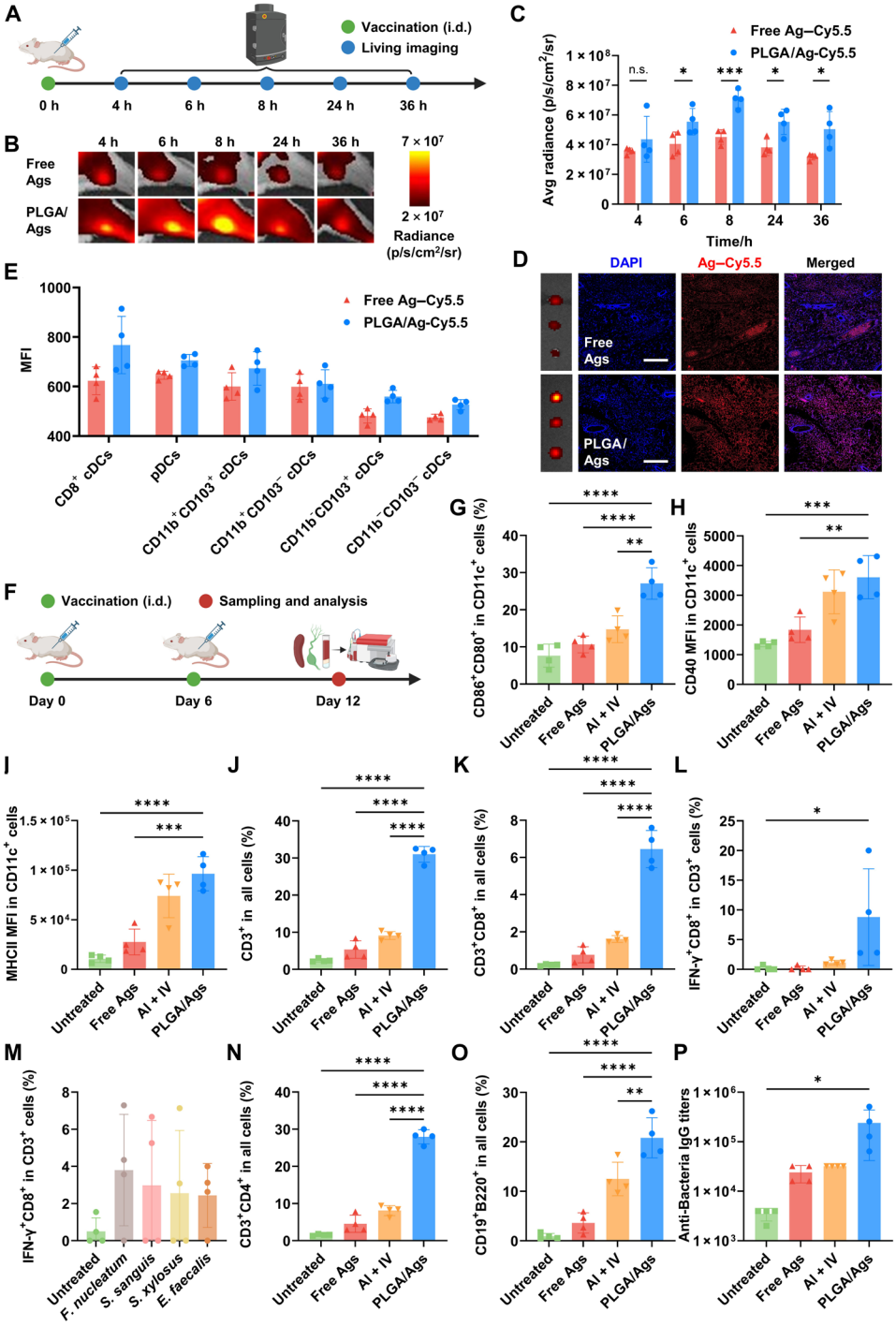

Fig. 4. In vivo immune stimulation by PLGA/Ag nanovaccine. (**A**) Schematic and timeline depicting the experimental design to evaluate the ability of PLGA/Ags to accumulate in lymph nodes. i.d., intradermal. Created with BioRender.com. (**B**) In vivo time-lapse fluorescence images of dLNs in mice treated with free Ag–Cy5.5 or PLGA/Ag-Cy5.5. (**C**) Statistical analysis of average Cy5.5 fluorescence signals in dLNs of mice based on images in (B). (**D**) Confocal fluorescence images of dLNs in mice treated with free Ag–Cy5.5 or PLGA/Ag-Cy5.5 (scale bars, 250 μm). (**E**) MFI of Cy5.5 in DC subsets from dLNs in mice treated with free Ag–Cy5.5 or PLGA/Ag-Cy5.5. cDCs, conventional DCs; pDCs, plasmacytoid DCs. (**F**) Schematic and timeline illustrating the experimental design to evaluate immune responses triggered by PLGA/Ags vaccine. (**G** to **I**) Expression levels of (G) CD80, CD86, (H) CD40, and (I) MHC II on DCs, indicating the maturation of DCs in the dLNs of mice injected with different vaccines. (**J** and **K**) Percentages of (J) $CD3^+$ and (K) $CD3^+CD8^+$ T cells in the dLNs of mice injected with different vaccines. (**L**) Percentages of IFN-γ^+CD8^+ T cells within $CD8^+$ T cells collected from mice in different groups after restimulated with bacterial Ags. (**M**) Percentages of IFN-γ^+CD8^+ T cells within $CD8^+$ T cells collected from mice treated with PLGA/Ags vaccines after restimulated with different bacterial Ags. (**N** and **O**) Percentages of (N) $CD3^+CD4^+$ T cells and (O) $CD19^+B220^+$ B cells in the dLNs of mice in different groups. (**P**) Anti-bacteria IgG titers in the serum of mice injected with different vaccines. All data are presented as means ± SD ($n = 4$). Statistical significance was calculated via unpaired *t* test (M) and one-way ANOVA [(G) to (P)] in GraphPad Prism. *$P < 0.05$; **$P < 0.01$; ***$P < 0.001$; ****$P < 0.0001$.

of mice receiving free Ag–Cy5.5 consistently remained low, potentially attributable to the lymphatic system's tendency to preferentially transport nanoparticles in the 100- to 200-nm-size range, while smaller, free proteins may bypass this mechanism (*43*).

Following the validation of the effective intralymphatic delivery of PLGA/Ags, we delved into the uptake of PLGA/Ags by APC) within dLNs. Confocal imaging of dLNs sections revealed that the Cy5.5 fluorescence signal was higher in the PLGA/Ag-Cy5.5 group compared to that in the free Ag–Cy5.5–treated group. Notably, regions exhibiting Cy5.5 fluorescence signal were devoid of 4′,6-diamidino-2-phenylindole (DAPI) fluorescence in the free Ag–Cy5.5–treated group, whereas, in the PLGA/Ag-Cy5.5–treated group, Cy5.5 fluorescence signals colocalized with DAPI signal, indicating that PLGA/Ags not only accumulate in dLNs but also proficiently convey Ags to APCs (Fig. 4D). To further dissect the dynamics of Ag uptake within dLNs, the specific DC subsets engaging in this process were further characterized using flow cytometry. As shown in Fig. 4E, it was observed that across DC subsets, more cells internalized the Ags in the PLGA/Ag-Cy5.5 group relative to the free Ag–Cy5.5–treated group. Intriguingly, in the PLGA/Ag-Cy5.5 group, $CD8^+$ conventional DCs, which play a crucial role in T cell activation and Ag internalization (*44*), followed by plasmacytoid DCs, which can rapidly secrete large amounts of interferon (IFN) in response to intracellular pathogen infections (*45*), internalized more Ags. In contrast, tolerogenic $CD11b^-CD103^+$ DCs internalized less Ags (*46*). This comprehensive evaluation underscored the proficiency of PLGA vaccine in not only reaching the dLNs but also in facilitating efficient Ag uptake by key immune players, paving the way for potent immune activation.

Subsequently, the maturation status of DCs in vivo prompted by the vaccine, along with other immune parameters, was validated using a murine model (Fig. 4F). The dLNs, spleens, and peripheral blood harvested from mice with two doses of vaccine (10 μg of Ag per mouse per dose) were processed into single-cell suspensions for comprehensive flow cytometry analysis (*47*). As anticipated, in comparison with the untreated group, the free Ags group, and the group receiving a traditional aluminum adjuvant combined with an inactivated bacterial vaccine (Al + IV), mice vaccinated with PLGA/Ags exhibited elevated expression levels of co-stimulatory molecule (CD80, CD86, CD40, and MHC II) on DCs within their dLNs (Fig. 4, G to I, and fig. S5A). Following this, the proportion of T cells in the dLNs, which are recipients of Ag presentation by DCs, was assessed (*41*). The results in Fig. 4J and fig. S5B indicated that T cells ($CD3^+$) were more abundant in mice vaccinated with PLGA/Ags compared to those in other groups. Given the intracellular nature of *F. nucleatum*, *S. sanguis*, *E. faecalis*, and *S. xylosus*, a strong cellular immune response is imperative to eradicate infected tumor cells and eliminate these bacteria (*11*, *23*, *48*). As shown in Fig. 4K and fig. S5C, the proportion of $CD8^+$ T cells was significantly higher in mice vaccinated with PLGA/Ags compared to that in other groups. To further confirm the Ag-specific cellular immune response of $CD8^+$ T cells, splenocytes from vaccinated mice were rechallenged with bacterial cell membranes in vitro. As expected, $CD8^+$ T cells from mice treated with PLGA/Ags secreted significantly higher levels of IFN-γ when stimulated with Ags from the four bacteria simultaneously, compared to other groups (Fig. 4L and fig. S5D). Meanwhile, $CD8^+$ T cells from PLGA/Ags-treated mice also produced substantial amounts of IFN-γ when stimulated with each bacterial Ag separately (Fig. 4M).

In addition to cellular immune response, humoral immunity also plays an important role in eliminating bacteria by neutralizing extracellular bacteria and those released from infected cells upon destruction with antibodies (*34*). As shown in Fig. 4 (N and O) and fig. S5 (E and F), the proportions of $CD4^+$ T cells and B cells ($CD19^+B220^+$) were significantly increased in mice vaccinated with PLGA/Ags. To directly quantify humoral immune activation, the antibody titers against bacterial Ags in the peripheral blood serum were quantified using enzyme-linked immunosorbent assay (ELISA) on Ag-coated plates. Mice vaccinated with PLGA/Ags exhibited significantly superior antibody production compared to the other groups (Fig. 4P). Thus, although the traditional aluminum adjuvant combined with inactivated vaccines enhanced DC activation when compared to free Ags, it showed limited efficiency in activating cellular immunity and humoral immunity. Conversely, the PLGA/Ags vaccine induced significantly stronger DC activation, as well as both cellular and humoral immune responses compared to the other groups. Given the strong stimulatory effect of PLGA/Ags, we further conducted a thorough biosafety evaluation. On day 6, after two rounds of vaccination, blood samples were collected for comprehensive hematological analysis, and major organ tissues were subjected to hematoxylin and eosin (H&E) staining for histopathological assessments. As shown in fig. S6A, all blood biochemistry and hematological parameters from mice vaccinated with PLGA/Ags remained within the normal reference range. Additionally, as shown in fig. S6B, no significant pathological changes were observed in the major organs of mice treated with PLGA/Ags. These results demonstrate that PLGA/Ags have negligible side effects on normal tissues and organs, supporting its excellent safety profile as a vaccine.

PLGA/Ags prevent cancer metastasis by eliminating intratumoral bacteria

To ascertain the therapeutic potential of PLGA/Ags in eradicating intratumoral bacteria and thwarting bacteria-induced tumor metastasis, investigative studies were expanded to encompass tumor-bearing mice models. The BALB/c mice were allocated into five distinct groups: (i) intravenous injection of luciferase-transfected 4T1 (4T1-Luc) tumor cells unafflicted by bacterial infection (uninfected); (ii) intravenous injection of tumor cells infected with a consortium of *F. nucleatum*, *E. faecalis*, *S. sanguis*, and *S. xylosus* (bacteria); (iii) intravenous injection of tumor cells with bacterial infection followed by treatment with free bacterial Ags (free Ags); (iv) intravenous injection of tumor cells with bacterial infection followed by vaccination with aluminum adjuvant and inactivated bacterial vaccine (Al + IV); and (v) intravenous injection of tumor cells with bacterial infection followed by vaccination with PLGA/Ags. Each mouse was injected with 2.5×10^5 4T1-Luc cells, with infected tumor cells at a multiplicity of infection (MOI) of 100, and the vaccine was administered at a dose of 10 μg of Ag per mouse. Once 4T1-Luc pulmonary metastases reach a certain size, they can emit bioluminescence upon exposure to luciferase substrates. In vivo imaging was performed at 6-day intervals to monitor the progression of pulmonary metastases (Fig. 5A). Consistent with the prior results, the data depicted in Fig. 5 (B and C) illustrated that mice in the bacteria group experienced abbreviated survival periods and accelerated metastatic dissemination compared to the uninfected group, confirming the potent tumor metastasis induced by *F. nucleatum*, *E. faecalis*, *S. sanguis*, and *S. xylosus*. Among the treatment groups, administration of free Ags was insufficient to prevent tumor metastasis. Similarly, the Al + IV treatment also did not appreciably curtail metastatic progression to levels akin to those observed in the

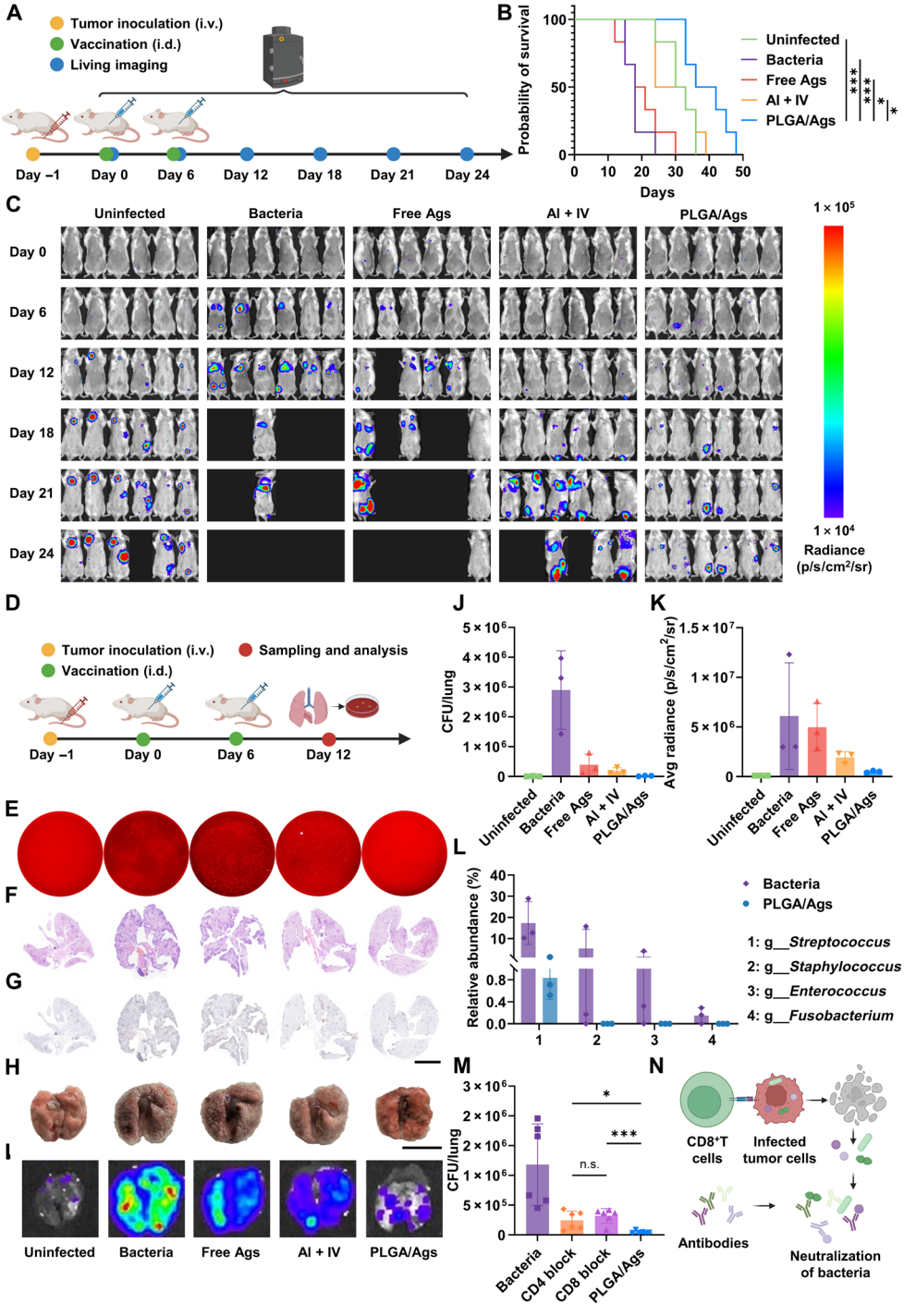

Fig. 5. PLGA/Ags overcoming bacteria-induced breast tumor metastasis. (**A**) Schematic and timeline illustrating the experimental design to evaluate the ability of PLGA/Ags in preventing bacteria-induced tumor metastasis. (**B**) Survival curves of mice in different groups ($n = 6$). (**C**) In vivo bioluminescence imaging to track the metastasis of 4T1-Luc cancer cells in mice with different treatments ($n = 6$). (**D**) Schematic and timeline showing the experimental design to evaluate the selective antibacterial activity of PLGA/Ags. i.v., intravenous. (**E**) Representative colony plate images showing the bacteria abundance in homogenized lungs of mice with different treatments. (**F** to **I**) Representative (F) hematoxylin and eosin (H&E) staining, (G) Ki-67 staining (scale bar, 4 mm), (H) gross morphology (scale bar, 1 cm), and (I) bioluminescence images of lungs in indicating different groups. (**J**) Colony-forming units (CFUs) quantifying bacteria abundance in homogenized lungs of mice after different treatments. Data are presented as means ± SD ($n = 3$). (**K**) Average bioluminescence signals of lungs in mice with different treatments. Data are presented as means ± SD ($n = 3$). (**L**) Relative abundance of lung microbiome in mice with or without PLGA/Ags treatment. Family-level taxonomy is presented as the percentage of total sequences ($n = 3$). (**M**) CFUs showing the bacteria abundance in homogenized lungs of mice with different treatments. Data are presented as the means ± SD ($n = 6$). n.s., not significant. (**N**) Schematic representation of cellular immunity and humoral immunity in clearing infected tumor cells and bacteria. Statistical significance was calculated via the log-rank (Mantel-Cox) test (B) and unpaired *t* test (C) in GraphPad Prism. $^*P < 0.05$; $^{***}P < 0.001$. (A), (D), and (N) created with BioRender.com.

absence of bacteria. In stark contrast, mice that received the PLGA/Ags vaccination exhibited significantly extended survival periods compared to the bacteria group, highlighting the pronounced efficacy of the PLGA/Ags vaccine in enhancing host resistance against bacteria-driven tumor progression and metastasis. Unexpectedly, the survival period of the PLGA/Ags-treated group even surpassed that of the uninfected group, which may be attributed to the fact that tumor cells infected with intracellular bacteria present bacterial peptides on their surface via MHC I molecules, making them susceptible to cytotoxic T cells that recognize bacterial epitopes generated by the vaccine, in addition to those that recognize tumor epitopes (*23*, *24*). Moreover, previous studies have demonstrated the presence of shared antigenic epitopes between host cells and bacteria, which could also contribute to the antitumor effects of the antibacterial vaccine (*49*). Therefore, PLGA/Ags not only eliminates specific bacteria to inhibit bacteria-driven tumor progression and metastasis but also enhances antitumor immune responses, thereby delaying the growth of cancer cells.

To comprehensively demonstrate the antibacterial effect of PLGA/Ags to delay the growth of tumor, a new round of treatment was conducted with the same experimental groups as described above (Fig. 5D). On the 12th day, all mice were euthanized, and their lungs were harvested for a series of analyses. As shown in Fig. 5 (E and J), the lung homogenate plating results indicated a reduction in lung bacterial colonies in the PLGA/Ags-treated mice, approaching levels observed in the uninfected group. As illustrated in Fig. 5 (F to H), H&E staining and Ki-67 staining of lung sections from the mice demonstrated substantially smaller dark tumor-indicative areas in the PLGA/Ags group compared to those in the bacteria group. This group also outperformed the free Ags group and the Al + IV group, nearly reaching the levels of the uninfected group. Lung images (Fig. 5H and fig. S7A) and bioluminescence imaging (Fig. 5, I and K, and fig. S7B) results corroborated these findings. To accurately reflect that the bacteria cleared by the vaccine were the tumor-associated *F. nucleatum*, *E. faecalis*, *S. sanguis*, and *S. xylosus*, bacterial community sequencing was performed on the lungs of the PLGA/Ags and bacteria groups. As shown in Fig. 5L and fig. S8, PLGA/Ags treatment effectively reduced the abundance of *Fusobacterium*, *Enterococcus*, *Streptococcus*, and *Staphylococcus* in the lungs of the mice. To investigate the role of humoral and cellular immunity, anti-CD4 or anti-CD8 antibodies were administered to mice during vaccination to block either humoral or cellular immunity. As shown in Fig. 5M and fig. S9, the bacterial count in the PLGA/Ags group was significantly lower compared to that in the CD4 block and CD8 block groups, indicating that both cellular and humoral immunity are essential components of the antibacterial immune response within tumors (Fig. 5N). Together, these experimental results indicate that the specific immunity induced by PLGA/Ags effectively eliminated *F. nucleatum*, *E. faecalis*, *S. sanguis*, and *S. xylosus* within tumor cells, thereby preventing the tumor lung metastasis induced by these bacteria.

Building on the above results, we further applied PLGA/Ags to a bacteria-induced CT-26 tumor metastasis model. On day −1, mice were intravenously injected with 2.5×10^5 CT-26-Luc cells, either infected or uninfected with bacteria, to establish the model. On days 0 and 6, the PLGA/Ags group was intradermally injected with a vaccine containing 10 μg of Ag. As shown in fig. S10 (A and B), *F. nucleatum*, *E. faecalis*, *S. sanguis*, and *S. xylosus* were also found to promote the metastasis of CT-26-Luc cancer cells. Tumor progression in bacteria-infected mice vaccinated with PLGA/Ags was significantly delayed compared to that in bacteria-infected mice and was also slightly delayed relative to uninfected mice. This result was consistent with observations from the 4T1-Luc model, further demonstrating that the immune response triggered by the antibacterial vaccine can effectively eliminate bacteria-infected tumor cells and delay cancer metastasis.

The long-term protective effect induced by PLGA/Ags

Breast cancer has a high propensity for both metastasis and recurrence, with recurrent tumors being particularly prone to further metastasis (*50*). Recent studies demonstrated that specific bacteria can induce tumor metastasis during the initial stage and also promote metastasis upon recurrence (*51*). Therefore, vaccines targeting intratumoral harmful bacteria must not only elicit a short-term immune response upon injection but also establish long-term immune memory effect to prevent bacteria from recolonizing recurrent tumor tissues and promoting tumor progression. Consequently, whether PLGA/Ags can induce long-term antibacterial immunity has emerged as a new area of interest. BALB/c mice were divided into two groups: (i) untreated, and (ii) PLGA/Ags (intradermally on days 0, 7, and 14). Each mouse received a vaccine dose containing 10 μg of Ag. Then, the blood samples were collected on days 7, 14, 28, and 42 (Fig. 6A). As shown in Fig. 6B, the Ag-specific immunoglobulin G (IgG) levels in blood serum, assessed by ELISA using plates coated with Ags from *F. nucleatum*, *S. sanguis*, *E. faecalis*, or *S. xylosus*, demonstrated that PLGA/Ags induced humoral immunity against all target bacteria. The total anti-bacteria IgG titers in the PLGA/Ags group were tracked over time, showing a gradual increase from days 7 to 28, followed by a decline (Fig. 6C). On day 42, peripheral blood was sampled to detect memory immune cells. As shown in Fig. 6 (D to F), significant increases were observed in both effector memory T cells ($CD44^{+-}$ $CD62L^{-}$) and central memory T cells ($CD44^{+}CD62L^{+}$) in mice vaccinated with PLGA/Ags. Additionally, the proportion of memory B cells ($CD19^{+}CD38^{-}$) in the vaccinated mice exhibited a significant increase (Fig. 6G).

Following three doses of PLGA/Ags vaccine, the mice were intravenous injected with 4T1-Luc cells infected with *F. nucleatum*, *S. sanguis*, *E. faecalis*, and *S. xylosus* (2.5×10^5 4T1-Luc cells per mouse, with an MOI of 100). Meanwhile, unvaccinated mice injected with infected or uninfected tumor cells were used as the control. The lung metastases were diligently tracked via the bioluminescence emitted by the luciferase with 6-day intervals (Fig. 6H). It was observed that three doses of PLGA/Ags effectively delayed the rate of pulmonary metastasis in bacteria-infected tumors, which is even a slower progression compared to that in tumors not infected with bacteria. Then, the mice were euthanized on day 55, the bioluminescence imaging (Fig. 6, I and L) and histological analysis of lungs (Fig. 6, J and K) further illustrated the antibacterial immune response induced by PLGA/Ags, preventing the progression of metastasis. In summary, in long-term immunity experiments, PLGA/Ags demonstrated its ability to establish effective immune memory, providing prolonged antibacterial protection and preventing bacteria-induced tumor metastasis. Moreover, this immune memory enhances the body's ability to eliminate bacteria-infected tumor cells more effectively than uninfected tumor cells.

DISCUSSION

In conclusion, this study developed a multivalent therapeutic antibacterial vaccine (PLGA/Ags) by encapsulating both soluble and

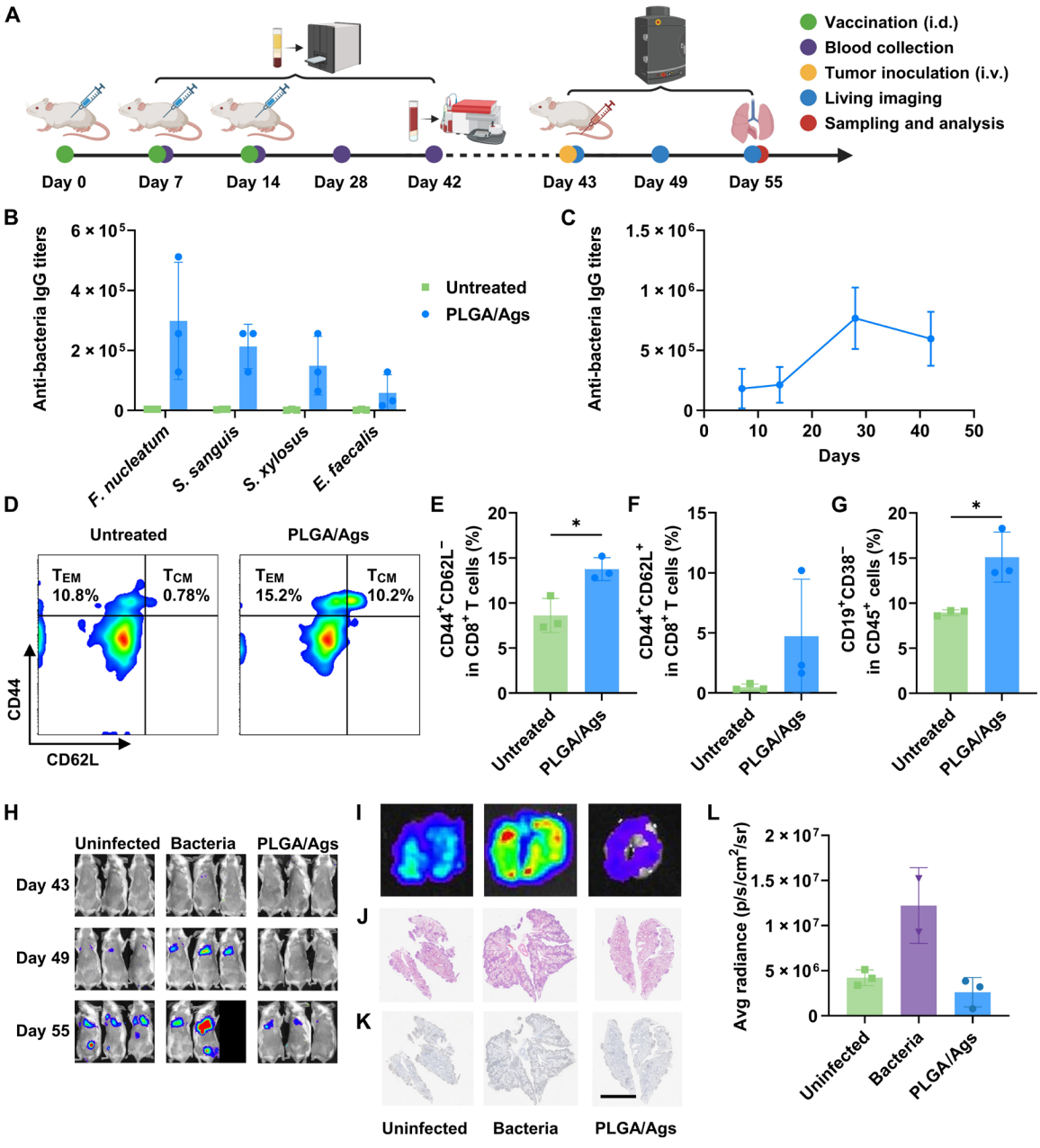

Fig. 6. Long-term immune memory induced by PLGA/Ags. (**A**) Schematic and timeline illustrating the experimental design to evaluate the ability of PLGA/Ags to induce immune memory effect in preventing bacteria-induced tumor metastasis. Created with BioRender.com. (**B**) IgG titers in the serum of mice with or without PLGA/Ags vaccine treatment against different bacteria. Data are presented as means ± SD ($n = 3$). (**C**) Anti-bacteria IgG titers in the serums of mice injected with PLGA/Ags vaccines. Data are presented as means ± SEM ($n = 3$). (**D** to **F**) Representative flow cytometric plots (D) and statistical analysis of (E) effector memory T cells (T_{EM}) ($CD44^+CD62L^-$) and (F) central memory T cells (T_{CM}) ($CD44^+CD62L^+$) within $CD8^+$ T cells of mice with or without PLGA/Ags vaccine treatment. Data are presented as means ± SD ($n = 3$). (**G**) $CD19^+CD38^-$ memory B cells within $CD45^+$ lymphocytes of mice with or without PLGA/Ags vaccine treatment. Data are presented as means ± SD ($n = 3$). (**H**) In vivo bioluminescence imaging to track metastasis of 4T1-Luc cancer cells in mice with different treatments ($n = 3$). (**I** to **K**) Representative (I) bioluminescence images, (J) H&E staining slides, and (K) Ki-67 staining slides (scale bar, 5 mm) of lungs in different groups. (**L**) Average bioluminescence signals in the lungs of mice with different treatments. Data are presented as means ± SD ($n = 3$ for uninfected group and PLGA/Ags group and $n = 2$ for the bacteria group due to mouse mortality). Statistical significance was calculated via unpaired *t* test (E) and (G) in GraphPad Prism. *$P < 0.05$.

insoluble fractions of lysates from *F. nucleatum*, *S. sanguis*, *E. faecalis*, and *S. xylosus* within PLGA nanoparticles. This vaccine aims to selectively eliminate these bacteria and tumor cells infected by them, thereby preventing bacteria-induced breast cancer metastasis. It helps prevent damage to normal microbiota and the development of antibiotic-resistant bacteria, which can result from the prolonged use of antibiotics to eliminate intratumoral bacteria. PLGA/Ags carry a rich array of Ags, enabling the immune system to comprehensively recognize the four target bacteria, and elicit a robust cellular immune response, allowing cytotoxic T cells to kill tumor cells infected with the target bacteria. The vaccine demonstrated significant efficacy in both the treatment and prevention of breast cancer lung metastasis models. It not only counteracted the tumor-promoting effects of the bacteria but also slowed tumor progression in vaccinated, bacteria-infected mice compared to that in uninfected mice. This study demonstrates that modulating the tumor microbiome with an antibacterial vaccine can combat breast cancer metastasis, highlighting the critical role of the tumor microbiome in cancer therapy. As more tumor-associated microbial species are identified, this vaccine platform can be adapted to selectively eliminate bacteria detrimental to cancer treatment while sparing beneficial ones, providing diverse solutions for various cancer types. Additionally, this study suggests that intratumoral bacteria could serve as targets for antitumor strategies, offering a perspective for developing innovative cancer therapies with potential clinical value.

MATERIALS AND METHODS

Materials, bacterial strains, cells, and animals

PLGA with *M*w of 12,000 to 15,000 (ester terminated, 50:50) was purchased from J&K Scientific. Poly(vinyl alcohol) (PVA; 80% hydrolyzed, *M*w of 9000 to 10,000) was obtained from Sigma-Aldrich. *F. nucleatum* [American Type Culture Collection (ATCC), 25586] was acquired from the China General Microbiological Culture Collection Center and cultured in thiolglycollate broth in an anaerobic environment. *E. faecalis* (ATCC, 29212) was procured from the Guangdong Microbial Culture Collection Center and cultured in brain heart infusion broth medium. *S. sanguis* (ATCC, 10556) was also obtained from the Guangdong Microbial Culture Collection Center and cultured in thiolglycollate medium. *S. xylosus* (ATCC, 29971) was sourced from the same center and cultured in Luria-Bertani medium. All bacterial solid culture media were prepared using Columbia blood agar. All media for bacteria culture were purchased from Qingdao Hope Bio-Technology Co. Ltd.

4T1-Luc cells were obtained from Shanghai Genechem Co. Ltd. and were cultured in RPMI 1640 medium (6016011, Dakewe Biotech) containing 10% fetal bovine serum (FBS) (JYK-FBS-301, Inner Mongolia Jin Yuan Kang Biotechnology Co. Ltd.) and 1% penicillin/streptomycin (PB180120, Pricella Life Science &Technology Co. Ltd.) at 37°C in 5% CO_2. BMDCs were prepared from C57BL/6 mice, and cultured in RPMI 1640 medium supplemented with 10% FBS, 1% penicillin/streptomycin, 0.1% β-mercaptoethanol, 0.01% granulocyte-macrophage colony-stimulating factor (CK-02, Novoprotein, Shanghai, China) and 0.01% IL-4 (HA210902, HUABIO). DC2.4 cells was purchased from Pricella Life Science & Technology Co. Ltd.

Six- to 8-week female BALB/c mice and 6- to 8-week C57BL/6 mice were purchased from Changzhou Cavens Laboratory Animal Co. Ltd. All animal experiments were performed in compliance with the relevant laws and approved by the Institutional Animal Care and Use Committee of Soochow University (no. SUDA20240724A01).

Bacterial Lysate Preparation

F. nucleatum, *E. faecalis*, *S. sanguis*, and *S. xylosus* were cultured at 37°C for 48 hours. Subsequently, bacterial cells were harvested by centrifugation at 10,000*g* for 10 min, followed by three sequential washes with PBS. The bacteria from each 50 ml of culture medium were then resuspended in 1 ml of 8 M urea solution and underwent sonication using a Sonic Dismembrator for 30 min on ice (sonication cycle: $T_{on} = 3$ s and $T_{off} = 5$ s; ultrasonic power of 500 W). Following ultrasonication, the suspensions were centrifuged at 10,000*g* and 4°C for 10 min, and the resulting supernatants were collected. The protein concentration of bacterial lysates was determined using BCA protein assay kit (AKPR017, Beijing Boxbio Science & Technology Co. Ltd.). The protein compositions were then analyzed by SDS-PAGE (EC0022-A, Shandong Sparkjade Biotechnology Co.) and stained by Coomassie brilliant blue.

Synthesis and characterization of PLGA/Ags

The PLGA nanoparticles were synthesized by the double-emulsion method. Briefly, 0.3 ml of bacterial lysate supernatant (protein at 1 mg/ml for each bacterial type) was added to 1 ml of dichloromethane solution containing PLGA (5 mg/ml). This mixture was homogenized by ultrasound to generate a water-in-oil (W/O) emulsion. Then, 1.3 ml of the W/O emulsion was added to 2.5 ml of 4% PVA solution and further homogenized by ultrasound again to form a water-in-oil-in-water (W/O/W) emulsion. The resulting 3.8 ml of W/O/W emulsion was then added to 6 ml of 1% PVA solution and stirred for 12 hours at room temperature, allowing the organic solvent to evaporate. The nanoparticles were then collected by centrifugation at 20,000*g* for 30 min, resuspended in 1 ml of 4% sucrose solution, and lyophilized for 48 hours. Before administration, the lyophilized PLGA nanoparticles were reconstituted in endotoxin-free PBS.

The hydrodynamic size of the PLGA nanoparticles was measured by Zetasizer Nano ZS (Malvern Instruments). TEM images were acquired using an FEI Tecnai G2 F20 Transmission Electron Microscope, using a 200-kV acceleration voltage.

Maturation of BMDC in vitro

As previously described, BMDCs obtained from C57BL/6 mice were initially seeded at a density of 1×10^6 cells per well in untreated round-bottom 24-well plates. Subsequently, 10 μl of PBS, PLGA nanoparticles (protein concentration of 4 mg/ml), bacterial lysate (protein concentration of 4 mg/ml), or 2 μl of LPS solution (1 mg/ml) was added to each well. After 12 hours incubation, cells from each well were collected by centrifugation at 1500*g* for 3 min and resuspended in PBS containing 1% FBS. The cells were then stained with anti–CD11c-FITC (117306, BioLegend), anti–CD86–phycoerythrin (PE) (159204, BioLegend), and anti–CD80-allophycocyanin (APC) (104714, BioLegend) and analyzed using flow cytometry on a BD Accuri C6 Plus. The supernatants were assessed for cytokine concentrations using TNF-α (SEKM-0034, Beijing Solarbio Science & Technology Co. Ltd.), IL-6 (SEKM-0007, Beijing Solarbio Science & Technology Co. Ltd.), and IL-12p70 (BMS6004, Invitrogen) ELISA kits.

Cellular uptake and Ag presentation in vitro

DC2.4 cells were seeded at a density of 10^6 cells per well in a 12-well plate containing coverslips. After 4 hours of incubation, 0.1 ml of

FITC-labeled bacterial protein (0.4 mg/ml), either in its free form or encapsulated in PLGA nanoparticles, was added to the corresponding wells and incubated for 4, 8, 12, and 24 hours. For confocal imaging, cells on each coverslip were fixed with 0.5 ml of 4 wt % paraformaldehyde solution to preserve cell morphology, followed by staining with 1 ml of 75 nM LysoTracker Red and 0.5 ml of DAPI (1 μg/ml) for 30 min. After staining, the coverslips were thoroughly washed and mounted onto glass slides. Imaging was performed using a Zeiss LSM 800 confocal laser scanning microscope. For flow cytometry, the incubated cells were digested with 0.25% trypsin for 3 min and collected by centrifugation at 1200 rpm for 3 min. The cells were then washed, and the FITC fluorescence intensity of each group was measured using a BD Accuri C6 Plus flow cytometer.

Enrichment of nanoparticles in lymph nodes

BALB/c mice were intradermally injected with an equivalent amount of Cy5.5 (A8103, APExBIO, Houston, USA.)–labeled bacteria proteins, encapsulated either in PLGA nanoparticles or in free form. To track the fluorescence signals of the bacterial proteins, mice were imaged by PerkinElmer IVIS Lumina III imaging system at 4-, 6-, 8-, 24-, and 36-hour time points postinjection. Following imaging, the mice were euthanized and the inguinal lymph nodes were harvested. For confocal imaging, the lymph nodes were embedded in paraffin, sectioned, stained with DAPI, and observed under a ZEISS LSM 800 confocal microscope. For flow cytometry analysis, the lymph nodes were homogenized, filtered through a 200-mesh to obtain single-cell suspensions, and divided into three groups for staining: group 1: stained with anti–CD11c-FITC (117306, BioLegend), anti–CD8a-PE (162304, BioLegend), and anti–CD11b-peridinin-chlorophyll-protein complex (PerCP) (101230, BioLegend); group 2: stained with anti–CD11c-FITC (117306, BioLegend), anti–CD103-APC (110906, BioLegend), and anti–CD11b-PerCP (101230, BioLegend); and group 3: stained with anti–CD11c-FITC (117306, BioLegend), anti–CD11b-PE (101208, BioLegend), and anti–B220-PerCP (103234, BioLegend). All stained cell suspensions were analyzed using a BD Accuri C6 Plus flow cytometer.

Immunological evaluation in vivo

To investigate the immune responses mouse model, inguinal LNs of mice with different treatments were collected, homogenized, and filtered through a 200-mesh to obtain single-cell suspensions. These suspensions were divided into four groups for flow cytometry analysis: group 1: stained with anti–CD11c-FITC (117306, BioLegend), anti–CD80-PE (104708, BioLegend), and anti–CD86-APC (159216, BioLegend); group 2: stained with anti–CD11c-FITC (117306, BioLegend), anti–I-A/I-E-PE (107608, BioLegend), and anti–CD40-PerCP (124624, BioLegend); group 3: stained with anti–CD3-FITC (100204, BioLegend), anti–CD45-PerCP (103130, BioLegend), anti–CD8a-PE (162304, BioLegend), and anti–CD4-APC (100412, BioLegend); group 4: stained with anti–CD19-FITC (152404, BioLegend) and anti–B220-PerCP (103234, BioLegend). All groups were analyzed using a BD Accuri C6 Plus flow cytometer.

To assess the specific humoral immune response, IgG levels were quantified using ELISA. Specifically, lysate of *F. nucleatum*, *S. sanguis*, *E. faecalis*, and *S. xylosus* (protein concentration of 40 μg/ml) was used to coat the ELISA plates. Ag-specific IgG concentrations in the serum were assessed using a series of twofold serial dilutions. The horseradish peroxidase goat anti-mouse IgG (H+L) antibody (K1221) was purchased from APExBIO, Houston, USA. The endpoint titers were presented as the sample dilution, yielding an optical density at 450 nm value double the level observed in the control serum.

To study the specific cellular immune response, mouse spleens were collected, homogenized, and filtered through a 200-mesh to obtain single-cell suspensions. Red blood cells (RBCs) were lysed using RBC lysis buffer, and splenocytes were collected by centrifugation at 1500*g* for 3 min. To assess Ag responsiveness, 1×10^6 splenocytes from each mouse were co-incubated with 1 μg of bacterial Ag in a 24-well plate for 24 hours. After incubation, the splenocytes were collected, resuspended in PBS containing 1% FBS, and stained with anti–CD3-FITC (100204, BioLegend) and anti–CD8a-PE (162304, BioLegend). The cells were then fixed, permeabilized, stained by anti–IFN-γ–APC (505809, BioLegend), and analyzed using a BD Accuri C6 Plus flow cytometer.

To investigate the immune memory response, the number of memory T cells in peripheral blood was measured. Blood samples were treated with RBC lysis solution, and lymphocytes were collected by centrifugation at 1500*g* for 3 min and resuspended in PBS containing 1% FBS. The lymphocytes were stained by anti–CD3-FITC (100204, BioLegend), anti–CD8a-PerCP (100732, BioLegend), anti–CD44-PE (103007, BioLegend), and anti–CD62L-APC (104412, BioLegend) and analyzed using flow cytometry on a BD Accuri C6 Plus.

Therapeutic efficiency of PLGA/Ags in inhibiting tumor metastasis

For the antitumor metastasis experiment, BALB/c mice were injected with 2.5×10^5 4T1-Luc cells infected with *F. nucleatum*, *S. sanguis*, *E. faecalis*, and *S. xylosus* (each at an MOI of 100) on day −1 to establish a bacteria-induced breast cancer metastasis model. Subsequently, the mice received intradermal injections of 50 μl of a vaccine containing Ag (0.2 mg/ml) on days 0 and 6. In monitoring the inhibitory effects of PLGA/Ags on metastatic tumor growth, the mice were intraperitoneally injected with 0.25 ml of luciferase substrate (15 mg/ml) for bioluminescence imaging using the PerkinElmer IVIS Lumina III imaging system every 3 days.

For the prevention of recurrence and metastasis experiment, each BALB/c mouse received an intradermal injection of 50 μl of vaccine containing Ags (0.2 mg/ml) on days 0, 7, and 14. On day 43, the mice were intravenously injected with 2.5×10^5 4T1-Luc cells infected with *F. nucleatum*, *S. sanguis*, *E. faecalis*, and *S. xylosus* (each at an MOI of 100). Every 6 days, the mice were intraperitoneally injected with 0.25 ml of luciferase substrate (15 mg/ml) for bioluminescence imaging using the PerkinElmer IVIS Lumina III imaging system.

Colony-forming unit counting assay

To evaluate the antibacterial capability, the level of bacteria load in the lungs with tumor metastasis was quantified. Specifically, lung samples were homogenized, diluted 1:1000, and spread onto Columbia blood agar plates. The plates were then incubated at 37°C for 2 days, after which the bacterial colonies were counted.

Statistical analysis

All statistical analyses were evaluated by GraphPad Prism (Prism 8.3.0; GraphPad Software, 2019). Two-tailed Student's *t* test was used for two-group comparisons, and one-way analysis of variance (ANOVA) with a Tukey's post hoc test was used for multiple comparisons. The threshold for statistical significance was $^*P < 0.05$,

$^{**}P < 0.01$, $^{***}P < 0.001$, and $^{****}P < 0.0001$. All figure illustrations were created with BioRender.com.

Supplementary Materials

This PDF file includes:

Figs. S1 to S10
Table S1

REFERENCES AND NOTES

1. R. L. Siegel, K. D. Miller, N. S. Wagle, A. Jemal, Cancer statistics, 2023. *CA Cancer J. Clin.* **73**, 17–48 (2023).
2. S. C. Smith, D. Theodorescu, Learning therapeutic lessons from metastasis suppressor proteins. *Nat. Rev. Cancer* **9**, 253–264 (2009).
3. B. Weigelt, J. L. Peterse, L. J. van't Veer, Breast cancer metastasis: Markers and models. *Nat. Rev. Cancer* **5**, 591–602 (2005).
4. H. Cao, Z. Dan, X. He, Z. Zhang, H. Yu, Q. Yin, Y. Li, Liposomes coated with isolated macrophage membrane can target lung metastasis of breast cancer. *ACS Nano* **10**, 7738–7748 (2016).
5. J. A. Gilbert, M. J. Blaser, J. G. Caporaso, J. K. Jansson, S. V. Lynch, R. Knight, Current understanding of the human microbiome. *Nat. Med.* **24**, 392–400 (2018).
6. D. Nejman, I. Livyatan, G. Fuks, N. Gavert, Y. Zwang, L. T. Geller, A. Rotter-Maskowitz, R. Weiser, G. Mallel, E. Gigi, A. Meltser, G. M. Douglas, I. Kamer, V. Gopalakrishnan, T. Dadosh, S. Levin-Zaidman, S. Avnet, T. Atlan, Z. A. Cooper, R. Arora, A. P. Cogdill, M. A. W. Khan, G. Ologun, Y. Bussi, A. Weinberger, M. Lotan-Pompan, O. Golani, G. Perry, M. Rokah, K. Bahar-Shany, E. A. Rozeman, C. U. Blank, A. Ronai, R. Shaoul, A. Amit, T. Dorfman, R. Kremer, Z. R. Cohen, S. Harnof, T. Siegal, E. Yehuda-Shnaidman, E. N. Gal-Yam, H. Shapira, N. Baldini, M. G. I. Langille, A. Ben-Nun, B. Kaufman, A. Nissan, T. Golan, M. Dadiani, K. Levanon, J. Bar, S. Yust-Katz, I. Barshack, D. S. Peeper, D. J. Raz, E. Segal, J. A. Wargo, J. Sandbank, N. Shental, R. Straussman, The human tumor microbiome is composed of tumor type-specific intracellular bacteria. *Science* **368**, 973–980 (2020).
7. B. A. Helmink, M. A. W. Khan, A. Hermann, V. Gopalakrishnan, J. A. Wargo, The microbiome, cancer, and cancer therapy. *Nat. Med.* **25**, 377–388 (2019).
8. L. Yang, A. Li, Y. Wang, Y. Zhang, Intratumoral microbiota: Roles in cancer initiation, development and therapeutic efficacy. *Signal Transduct. Target. Ther.* **8**, 35 (2023).
9. J. B. Xavier, V. B. Young, J. Skufca, F. Ginty, T. Testerman, A. T. Pearson, P. Macklin, A. Mitchell, I. Shmulevich, L. Xie, J. G. Caporaso, K. A. Crandall, N. L. Simone, F. Godoy-Vitorino, T. J. Griffin, K. L. Whiteson, H. H. Gustafson, D. J. Slade, T. M. Schmidt, M. R. S. Walther-Antonio, T. Korem, B. M. Webb-Robertson, M. P. Styczynski, W. E. Johnson, C. Jobin, J. M. Ridlon, A. Y. Koh, M. Yu, L. Kelly, J. A. Wargo, The cancer microbiome: Distinguishing direct and indirect effects requires a systemic view. *Trends Cancer* **6**, 192–204 (2020).
10. L. Parhi, T. Alon-Maimon, A. Sol, D. Nejman, A. Shhadeh, T. Fainsod-Levi, O. Yajuk, B. Isaacson, J. Abed, N. Maalouf, A. Nissan, J. Sandbank, E. Yehuda-Shnaidman, F. Ponath, J. Vogel, O. Mandelboim, Z. Granot, R. Straussman, G. Bachrach, Breast cancer colonization by *Fusobacterium nucleatum* accelerates tumor growth and metastatic progression. *Nat. Commun.* **11**, 3259 (2020).
11. A. Fu, B. Yao, T. Dong, Y. Chen, J. Yao, Y. Liu, H. Li, H. Bai, X. Liu, Y. Zhang, C. Wang, Y. Guo, N. Li, S. Cai, Tumor-resident intracellular microbiota promotes metastatic colonization in breast cancer. *Cell* **185**, 1356–1372 e26 (2022).
12. L. Chen, J. Shen, Z. Kang, Z. Zhang, Z. Zheng, L. Zhang, Z. Xiao, Q. Zhang, H. Fang, J. Zhou, Y. Wang, Y. Yang, Z. Liu, Q. Chen, *Fusobacterium nucleatum*-mimicking nanovehicles to overcome chemoresistance for breast cancer treatment by eliminating tumor-colonizing bacteria. *Chem* **10**, 1783–1803 (2024).
13. C. Nathan, Antibiotics at the crossroads. *Nature* **431**, 899–902 (2004).
14. L. Chen, R. Zhao, J. Shen, N. Liu, Z. Zheng, Y. Miao, J. Zhu, L. Zhang, Y. Wang, H. Fang, J. Zhou, M. Li, Y. Yang, Z. Liu, Q. Chen, Antibacterial *Fusobacterium nucleatum*-mimicking nanomedicine to selectively eliminate tumor-colonized bacteria and enhance immunotherapy against colorectal cancer. *Adv. Mater.* **35**, e2306281 (2023).
15. M.-H. Xiong, Y. Bao, X.-Z. Yang, Y.-H. Zhu, J. Wang, Delivery of antibiotics with polymeric particles. *Adv. Drug Deliv. Rev.* **78**, 63–76 (2014).
16. D. Raggi, M. Bandini, F. Pederzoli, P. Giannatempo, L. Marandino, G. Basile, A. Gallina, A. Briganti, F. Montorsi, A. Necchi, Concomitant antibiotics (ATBs) use and survival outcomes in patients (pts) with muscle-invasive bladder cancer (MIBC) treated with neoadjuvant pembrolizumab (PURE-01 study). *J. Clin. Oncol.* **39**, 449 (2021).
17. T. Hagan, M. Cortese, N. Rouphael, C. Boudreau, C. Linde, M. S. Maddur, J. Das, H. Wang, J. Guthmiller, N.-Y. Zheng, M. Huang, A. A. Uphadhyay, L. Gardinassi, C. Petitdemange, M. P. McCullough, S. J. Johnson, K. Gill, B. Cervasi, J. Zou, A. Bretin, M. Hahn, A. T. Gewirtz, S. E. Bosinger, P. C. Wilson, S. Z. Li, G. Alter, S. Khurana, H. Golding, B. Pulendran, Antibiotics-driven gut microbiome perturbation alters immunity to vaccines in humans. *Cell* **178**, 1313–1328.e13 (2019).
18. L. Chen, R. Zhao, Z. Kang, Z. Cao, N. Liu, J. Shen, C. Wang, F. Pan, X. Zhou, Z. Liu, Y. Yang, Q. Chen, Delivery of short chain fatty acid butyrate to overcome Fusobacterium nucleatum-induced chemoresistance. *J. Control. Release* **363**, 43–56 (2023).
19. L. Derosa, B. Routy, L. Zitvogel, A. M. Thomas, G. Zalcman, S. Friard, J. Mazieres, C. Audigier-Valette, D. Moro-Sibilot, F. Goldwasser, C. Richard, F. Ghiringhelli, F. Barlesi, A. Elkrief, C. A. C. Silva, D. Planchard, N. Segata, S. Martinez, J. C. Soria, B. Besse, Intestinal *Akkermansia muciniphila* predicts overall survival in advanced non-small cell lung cancer patients treated with anti-PD-1 antibodies: Results a phase II study. *J. Clin. Oncol.* **39**, 9019–9019 (2021).
20. B. Routy, E. Le Chatelier, L. Derosa, C. P. M. Duong, M. T. Alou, R. Daillere, A. Fluckiger, M. Messaoudene, C. Rauber, M. P. Roberti, M. Fidelle, C. Flament, V. Poirier-Colame, P. Opolon, C. Klein, K. Iribarren, L. Mondragon, N. Jacquelot, B. Qu, G. Ferrere, C. Clemenson, L. Mezquita, J. R. Masip, C. Naltet, S. Brosseau, C. Kaderbhai, C. Richard, H. Rizvi, F. Levenez, N. Galleron, B. Quinquis, N. Pons, B. Ryffel, V. Minard-Colin, P. Gonin, J. C. Soria, E. Deutsch, Y. Loriot, F. Ghiringhelli, G. Zalcman, F. Goldwasser, B. Escudier, M. D. Hellmann, A. Eggermont, D. Raoult, L. Albiges, G. Kroemer, L. Zitvogel, Gut microbiome influences efficacy of PD-1-based immunotherapy against epithelial tumors. *Science* **359**, 91–97 (2018).
21. J. H. Kwon, W. G. Powderly, The post-antibiotic era is here. *Science* **373**, 471 (2021).
22. K. Kingwell, Vaccines take a shot at antimicrobial resistance. *Nat. Rev. Drug Discov.* **17**, 229–231 (2018).
23. S. Kalaora, A. Nagler, D. Nejman, M. Alon, C. Barbolin, E. Barnea, S. L. C. Ketelaars, K. Cheng, K. Vervier, N. Shental, Y. Bussi, R. Rotkopf, R. Levy, G. Benedek, S. Trabish, T. Dadosh, S. Levin-Zaidman, L. T. Geller, K. Wang, P. Greenberg, G. Yagel, A. Peri, G. Fuks, N. Bhardwaj, A. Reuben, L. Hermida, S. B. Johnson, J. R. Galloway-Pena, W. C. Shropshire, C. Bernatchez, C. Haymaker, R. Arora, L. Roitman, R. Eilam, A. Weinberger, M. Lotan-Pompan, M. Lotem, A. Admon, Y. Levin, T. D. Lawley, D. J. Adams, M. P. Levesque, M. J. Besser, J. Schachter, O. Golani, E. Segal, N. Geva-Zatorsky, E. Ruppin, P. Kvistborg, S. N. Peterson, J. A. Wargo, R. Straussman, Y. Samuels, Identification of bacteria-derived HLA-bound peptides in melanoma. *Nature* **592**, 138–143 (2021).
24. R. Naghavian, W. Faigle, P. Oldrati, J. Wang, N. C. Toussaint, Y. Qiu, G. Medici, M. Wacker, L. K. Freudenmann, P. E. Bonte, M. Weller, L. Regli, S. Amigorena, H. G. Rammensee, J. S. Walz, S. D. Brugger, M. Mohme, Y. Zhao, M. Sospedra, M. C. Neidert, R. Martin, Microbial peptides activate tumour-infiltrating lymphocytes in glioblastoma. *Nature* **617**, 807–817 (2023).
25. R. Zander, D. Schauder, G. Xin, C. Nguyen, X. Wu, A. Zajac, W. Cui, $CD4^+$ T cell help is required for the formation of a cytolytic $CD8^+$ T cell subset that protects against chronic infection and cancer. *Immunity* **51**, 1028–1042.e4 (2019).
26. F. Chen, M. Zhang, F. Yang, L. Wang, J. Liu, J. Liu, Y. Pang, Dual-antigen-displaying nanovaccines elicit synergistic immunoactivation for treating cancer and preventing infectious complications. *Small* **20**, e2307748 (2024).
27. D. S. Wilson, S. Hirosue, M. M. Raczy, L. Bonilla-Ramirez, L. Jeanbart, R. Wang, M. Kwissa, J. F. Franetich, M. A. S. Broggi, G. Diaceri, X. Quaglia-Thermes, D. Mazier, M. A. Swartz, J. A. Hubbell, Antigens reversibly conjugated to a polymeric glyco-adjuvant induce protective humoral and cellular immunity. *Nat. Mater.* **18**, 175–185 (2019).
28. J. J. Moon, H. Suh, A. Bershteyn, M. T. Stephan, H. Liu, B. Huang, M. Sohail, S. Luo, S. H. Um, H. Khant, J. T. Goodwin, J. Ramos, W. Chiu, D. J. Irvine, Interbilayer-crosslinked multilamellar vesicles as synthetic vaccines for potent humoral and cellular immune responses. *Nat. Mater.* **10**, 243–251 (2011).
29. C. J. Melief, S. H. van der Burg, Immunotherapy of established (pre)malignant disease by synthetic long peptide vaccines. *Nat. Rev. Cancer* **8**, 351–360 (2008).
30. M. Schnare, G. M. Barton, A. C. Holt, K. Takeda, S. Akira, R. Medzhitov, Toll-like receptors control activation of adaptive immune responses. *Nat. Immunol.* **2**, 947–950 (2001).
31. N. Petrovsky, Novel human polysaccharide adjuvants with dual Th1 and Th2 potentiating activity. *Vaccine* **24**, S6–S29 (2006).
32. K. K. Chereddy, V. L. Payen, V. Préat, PLGA: From a classic drug carrier to a novel therapeutic activity contributor. *J. Control. Release* **289**, 10–13 (2018).
33. G. P. Chen, T. Ushida, T. Tateishi, Hybrid biomaterials for tissue engineering: A preparative method for PLA or PLGA-collagen hybrid sponges. *Adv. Mater.* **12**, 455–457 (2000).
34. M. Super, E. J. Doherty, M. J. Cartwright, B. T. Seiler, F. Langellotto, N. Dimitrakakis, D. A. White, A. G. Stafford, M. Karkada, A. R. Graveline, C. L. Horgan, K. R. Lightbown, F. R. Urena, C. D. Yeager, S. A. Rifai, M. O. Dellacherie, A. W. Li, C. Leese-Thompson, H. Ijaz, A. R. Jiang, V. Chandrasekhar, J. M. Scott, S. L. Lightbown, D. E. Ingber, D. J. Mooney, Biomaterial vaccines capturing pathogen-associated molecular patterns protect against bacterial infections and septic shock. *Nat. Biomed. Eng.* **6**, 8–18 (2022).
35. L. Ma, L. Diao, Z. Peng, Y. Jia, H. Xie, B. Li, J. Ma, M. Zhang, L. Cheng, D. Ding, X. Zhang, H. Chen, F. Mo, H. Jiang, G. Xu, F. Meng, Z. Zhong, M. Liu, Immunotherapy and prevention of cancer by nanovaccines loaded with whole-cell components of tumor tissues or cells. *Adv. Mater.* **33**, e2104849 (2021).
36. K. B. Preston, T. W. Randolph, Stability of lyophilized and spray dried vaccine formulations. *Adv. Drug Deliv. Rev.* **171**, 50–61 (2021).

37. J. Hare, R. Hesselink, A. Bongers, P. Blakeley, G. Riggall, Improving vaccine equity by increasing vaccine thermostability. *Sci. Transl. Med.* **16**, eadm7471 (2024).
38. L. Chen, Z. Kang, J. Shen, R. Zhao, Y. Miao, L. Zhang, Z. Zheng, Z. Zhang, N. Liu, C. Wang, H. Fang, J. Zhou, Y. Wang, Z. Liu, Y. Yang, Q. Chen, An emerging antibacterial nanovaccine for enhanced chemotherapy by selectively eliminating tumor-colonizing bacteria. *Sci. Bull.* **69**, 2565–2579 (2024).
39. A. Gardner, B. Ruffell, Dendritic cells and cancer immunity. *Trends Immunol.* **37**, 855–865 (2016).
40. Q. Yin, W. Luo, V. Mallajosyula, Y. Bo, J. Guo, J. Xie, M. Sun, R. Verma, C. Li, C. M. Constantz, L. E. Wagar, J. Li, E. Sola, N. Gupta, C. Wang, O. Kask, X. Chen, X. Yuan, N. C. Wu, J. Rao, Y. H. Chien, J. Cheng, B. Pulendran, M. M. Davis, A TLR7-nanoparticle adjuvant promotes a broad immune response against heterologous strains of influenza and SARS-CoV-2. *Nat. Mater* **22**, 380–390 (2023).
41. Y. Miao, L. Niu, X. Lv, Q. Zhang, Z. Xiao, Z. Ji, L. Chen, Y. Liu, N. Liu, J. Zhu, Y. Yang, Q. Chen, A minimalist pathogen-like sugar nanovaccine for enhanced cancer immunotherapy. *Adv. Mater.* **36**, 2410715 (2024).
42. Y. Ding, Z. Li, A. Jaklenec, Q. Hu, Vaccine delivery systems toward lymph nodes. *Adv. Drug Deliv. Rev.* **179**, 113914 (2021).
43. Y.-N. Zhang, J. Lazarovits, W. Poon, B. Ouyang, L. N. M. Nguyen, B. R. Kingston, W. C. W. Chan, Nanoparticle size influences antigen retention and presentation in lymph node follicles for humoral immunity. *Nano Lett.* **19**, 7226–7235 (2019).
44. O. P. Joffre, E. Segura, A. Savina, S. Amigorena, Cross-presentation by dendritic cells. *Nat. Rev. Immunol.* **12**, 557–569 (2012).
45. B. Reizis, Plasmacytoid dendritic cells: Development, regulation, and function. *Immunity* **50**, 37–50 (2019).
46. V. Cerovic, C. C. Bain, A. M. Mowat, S. W. Milling, Intestinal macrophages and dendritic cells: What's the difference? *Trends Immunol.* **35**, 270–277 (2014).
47. J. R. Li, G. Wang, Z. Y. Wen, S. M. Sun, Z. H. Han, Y. Q. Yang, J. Wu, Z. F. Pei, L. Y. Liu, Y. D. Chen, L. Cheng, Modulating the electronic structure of MnNi2S3 nanoelectrodes to activate pyroptosis for electrocatalytic hydrogen-immunotherapy. *Adv. Mater* **36**, 2412925 (2024).
48. W. Li, Q.-W. Chen, J.-X. Fan, Z.-Y. Han, W.-F. Song, X. Zeng, X.-Z. Zhang, Bacterial biohybrids for invasion of tumor cells promote antigen cross-presentation through gap junction. *Adv. Mater* **36**, 2402532 (2024).
49. M. Wang, B. Rousseau, K. Qiu, G. Huang, Y. Zhang, H. Su, C. Le Bihan-Benjamin, I. Khati, O. Artz, M. B. Foote, Y. Y. Cheng, K.-H. Lee, M. Z. Miao, Y. Sun, P. J. Bousquet, M. Hilmi, E. Dumas, A. S. Hamy, F. Reyal, L. Lin, P. M. Armistead, W. Song, A. Vargason, J. C. Arthur, Y. Liu, J. Guo, X. Zhou, J. Nguyen, Y. He, J.-P. Ting, A. C. Anselmo, L. Huang, Killing tumor-associated bacteria with a liposomal antibiotic generates neoantigens that induce anti-tumor immune responses. *Nat. Biotechnol.* **42**, 1263–1274 (2024).
50. A. I. Riggio, K. E. Varley, A. L. Welm, The lingering mysteries of metastatic recurrence in breast cancer. *Br. J. Cancer* **124**, 13–26 (2021).
51. Y. Ma, H. Chen, H. Li, M. Zheng, X. Zuo, W. Wang, S. Wang, Y. Lu, J. Wang, Y. Li, J. Wang, M. Qiu, Intratumor microbiome-derived butyrate promotes lung cancer metastasis. *Cell Rep. Med.* **5**, 101488 (2024).

Acknowledgments: Figures were created with BioRender.com. **Funding:** This article was partially supported by the National Research Programs of China (2020YFA0211100 and 2022YFA1206500), the National Natural Science Foundation of China (52450010, 52325106, and 52271248), the Natural Science Foundation of Jiangsu Province (BK20240040), the Collaborative Innovation Center of Suzhou Nano Science and Technology, the Suzhou Key Laboratory of Nanotechnology and Biomedicine, and the 111 Program from the Ministry of Education of China. **Author contributions:** Conceptualization: Z.K., L.C., Q.C., and Y.Y. Methodology: Z.K., L.C., Q.C., Z.Z., Z.X., Y.M., and Y.Y. Software: L.C. and Y.Y. Validation: L.C. and Y.Y. Formal analysis: L.C., J.S., and Y.Y. Investigation: Z.K., L.C., P.L., J.S., and Y.Y. Resources: L.C. and Y.Y. Data curation: L.C. and Y.Y. Writing—original draft: Z.K., L.C., Q.C., and Y.Y. Writing—review and editing: Z.K., L.C., Q.C., P.L., Z.Z., Z.X., Y.M., and Y.Y. Visualization: L.C. and Y.Y. Supervision: Q.C. and Y.Y. Funding acquisition: Q.C. and Y.Y. **Competing interests:** The authors declare that they have no competing interest. **Data and materials availability:** All data needed to evaluate the conclusions in the paper are present in the paper and/or the Supplementary Materials.

Submitted 11 September 2024
Accepted 7 February 2025
Published 14 March 2025
10.1126/sciadv.adt0341